Smart sensing of damage in flexible plates through MEMS

Stefano Mariani*

Dipartimento di Ingegneria Civile e Ambientale,
Politecnico di Milano,
Piazza L. da Vinci 32, 20133 Milano, Italy
E-mail: stefano.mariani@polimi.it
*Corresponding author

Francesco Caimmi

Dipartimento di Chimica,
Politecnico di Milano,
Materiali e Ingegneria Chimica 'Giulio Natta',
Piazza L. da Vinci 32, 20133 Milano, Italy
E-mail: francesco.caimmi@polimi.it

Matteo Bruggi

Dipartimento di Ingegneria Civile e Ambientale,
Politecnico di Milano,
Piazza L. da Vinci 32, 20133 Milano, Italy
E-mail: matteo.bruggi@polimi.it

Paolo Bendiscioli

STMicroelectronics, MSH Division,
Via Tolomeo 1, 20010 Cornaredo, Italy
E-mail: paolo.bendiscioli@st.com

Abstract: In this work, we present a methodology to monitor the state of damage- or crack-containing flexible plates through low-cost, commercial off-the-shelf MEMS accelerometers. Under quasi-static, time-varying loading conditions we track the evolution of the damaged zone (e.g., the length of an inner crack) accounting for the drift in the compliance of the specimens, measured by means of the magnitude of the load-induced rotation at MEMS position. We then validate this health monitoring methodology, showing that it turns out to be sensitive to the damage and provides results in good accordance with theoretical findings. Next, we propose a technique to optimally deploy the MEMS sensors over the plate. Referring to an isotropic square plate containing damaged zones of reduced bending stiffness, we numerically investigate the sensitivity of the load-induced state (in terms of out-of-plane displacement and rotation of the normal to the mid-plane) to the position of the damaged area, and we adopt a constrained topology optimisation tool to determine the best sensor deployment to efficiently sense the damage.

Keywords: structural health monitoring; micro-electro-mechanical systems; MEMS; thin plates; damage.

Reference to this paper should be made as follows: Mariani, S., Caimmi, F., Bruggi, M. and Bendiscioli, P. (2014) 'Smart sensing of damage in flexible plates through MEMS', *Int. J. Mechanisms and Robotic Systems*, Vol. 2, No. 1, pp.67–95.

Biographical notes: Stefano Mariani received his MS (cum laude) in Civil Engineering in 1995, and his PhD in Structural Engineering in 1999, both from the Politecnico of Milan. He is currently an Associate Professor at the Department of Civil and Environmental Engineering, Politecnico of Milan. He is currently a member of the editorial boards of eight international journals. He has been recipient of the Associazione Carlo Maddalena Prize for graduate students (1996), and of the Fondazione Confalonieri Prize for PhD students (2000). His main research interests are: numerical simulations of ductile fracture in metals and quasi-brittle fracture in heterogeneous and functionally graded materials; extended finite element methods; calibration of constitutive models via extended and sigma-point Kalman filters; multi-scale solution methods for dynamic delamination in layered composites; reliability of MEMS subject to shocks and drops; and structural health monitoring of composite structures through MEMS sensors.

Francesco Caimmi received his Master in Materials Engineering at the Politecnico di Milano, in 2005 and his PhD in Materials Engineering in 2009 at the same university, where he currently holds a postdoctoral position. His research interests include fracture and failure of composite materials, and recently started working on structural health monitoring of composite structures.

Matteo Bruggi received his Laurea summa cum laude in Civil Engineering at the Università di Pavia in 2003, Master's in Reinforced Concrete Structures at Politecnico di Milano in 2004, and PhD in Civil Engineering at the Università di Pavia in 2008. He has been an Assistant Professor at Politecnico di Milano, Department of Civil and Environmental Engineering since 2011. He is an author of more than 25 papers published in international journals, mainly involved in the following research topics: topology optimisation, with particular interest in stress-constrained optimisation, design-dependent loads, incompressible media and micro-structured materials; automatic generation of optimal layouts of reinforcement through energy-based methods; numerical analysis of the cohesive crack growth in quasi-brittle materials; finite element modelling, with particular interest in truly-mixed discretisations based on the Hellinger-Reissner variational principle and in adaptive techniques.

Paolo Bendiscioli graduated in Electronic Engineering at the University of Pavia, Italy, in 1997 and he has been working since 1997 for STMicroelectronics. He is currently an Application Manager of the Motion MEMS Division.

1 Introduction

The detection of a potentially dangerous damage in structures exposed to accidental events and aging is becoming a timely field of research, see e.g., the recently published special issue on structural health monitoring, SHM (IEEE Sensors Journal, 2009). One of the main issues to be handled is the online detection of critical situations, so as to smartly manage the maintenance procedures.

Lightweight composite components, that constitute important parts of aeronautical and aerospace structures, can be exposed to accidental events (e.g., debris impacts) causing damage inception and subsequent growth (Abrate, 1998). Because of the composite microstructure, it is sometimes difficult to instantaneously detect such damage, which may consist in internal cracking (delamination) between adjacent plies (Mariani and Corigliano, 2005). Several attempts were made to monitor the health of composite laminates by embedding Bragg gratings (Tao et al., 2000) or piezoelectric sensors (Kumar et al., 2007). Whilst these sensors are known to be very accurate, their size can exceed the thickness of a single ply and the strain state in the surrounding region turns out to get varied. Moreover, the overall sensitivity of the composite to defects can be detrimentally affected. Hence, to monitor the health of a composite panel it appears that the composite itself gets exposed to premature failure events; this is obviously unacceptable from the structural reliability viewpoint.

In this work, we propose a SHM approach of a surface kind, with sensors glued to the outer skin of the structural component (in our experimental investigation, of the specimen). While the presence of the sensors can still affect the state of strain and stress inside the structural component, the distortion of the microstructure is avoided close to the interlaminar regions where the sensors are embedded and, therefore, the structural reliability is expected to be not detrimentally affected. The other way around, the exposure to the outer environment, especially in terms of temperature change, may lead to reliability issues of the SHM system itself; this aspect is beyond the scope of the present work, and will not be discussed here.

To be attractive for lightweight structures, i.e., for flexible plates and shells, sensors need to be light in weight as well. Self-monitoring composite structures can be obtained through a micro electro-mechanical system (MEMS)-based approach (Glaser and Tolman, 2008; Ratcliffe et al., 2008). Since MEMS sensors are pervasive, they can be used as surface monitoring systems without affecting the overall structural dynamics, even if they are deployed in very dense arrays.

Mechanical effects of ongoing damage phenomena need to be effectively sensed. Therefore, we first focused on the assessment of the capability of the SHM system to detect damage of known location and extent. In case of damaged area growing also in size, and thus not keeping a constant location, the performance of the SHM system may change in time; an accurate tracking of the structural state would then require a filter (or controller) to be adopted, thus allowing to identify size and location of the damaged area, along with the quantification of the damage itself (Corigliano and Mariani, 2004; Mariani and Ghisi, 2007).

With reference to a standard double-cantilever beam (DCB) test, we show experimental results and a theoretical interpretation of a very simple set-up, with a tri-axis MEMS accelerometer held fixed to the specimen to continuously monitor its health. Provided that instrument noises are accounted for, we show that MEMS

accelerometers are able to monitor in real time the length of the dominant crack (or delamination).

Then, we propose an approach to optimally deploy sensors all over the structure. With reference to thin plates, damage is assumed to consist of a local reduction of the bending stiffness, and methods of mathematical programming (Svanberg, 1987) are adopted to find the locations guaranteeing the maximum sensitivity to the damage with the minimal number of sensors used.

The remainder of this paper is thus organised as follows. In Section 2, we describe the offered SHM system, and provide details of the adopted MEMS sensors and monitoring scheme. Section 3 deals with the validation of the SHM scheme with composite plates subjected to cyclic tests: results are provided to compare the acquired experimental data with a simple theoretical description of the test, resting on Bernoulli-Euler beam bending. The problem of optimal deployment of the sensors is described in Section 4: an approach along the lines of topology optimisation is provided, and results are reported for simply supported, isotropic thin plates featuring localised damaged area. Finally, some concluding remarks and possible future developments are gathered in Section 5.

2 MEMS-based structural health monitoring

In the tests to be presented in Section 3, we used three-axis MEMS accelerometers to monitor potential changes in the structural health of flexible plates. In fact, no matter whether they are isotropic and homogeneous, under time-varying loadings such plates undergo displacement and rotation fields dependent on their geometry and health. In case of defective plates, e.g., because of areas with reduced bending stiffness or because of inner cracks (sometimes not visible from the outside), the aforementioned fields are expected to change if defects are growing. MEMS accelerometers, nowadays adopted for remote motion control in new game consoles, are able to feel the gravity direction; under quasi-static loadings, variations in the acceleration components can be exploited to sense local rotations (even if gyroscopes or inclinometers are actually devised to do that).

In the remainder of this section, we describe the features of the used MEMS sensor and of the monitoring scheme.

2.1 MEMS sensor

The sensing part of the SHM scheme was constituted by the commercial off-the-shelf LIS3LV02DQ three-axis, digital output MEMS accelerometer (STMicroelectronics, 2005), provided by STMicroelectronics together with its evaluation board. Due to the smooth and slowly time-varying (quasi-static) applied loading, the MEMS full scale was switched to ±2g, g being the gravity acceleration. Under such loading, we can assume that the structural damage evolves in a quasi-static fashion as well; focusing on the steady state-like effects of each load level (see the discussion in Section 3.5), and therefore disregarding the initial (potentially fast) transient stage, the bandwidth of 640 Hz featured by the MEMS proved enough to monitor the evolution of the specimen health. The sensitivity (around 1,000 LSb/g) and the resolution (1 mg) proved also sufficient for the present monitoring applications; on the other hand, the accuracy of the output needs to be checked in order to understand if the sensor can effectively recognise damage or crack evolution.

A thorough discussion on the (mechanical) sensing part of this family of micro-accelerometers and on their reliability can be found (e.g., in Mariani et al., 2007; 2009; Ghisi et al., 2009a, 2009b); readers are referred to those papers for additional details, less pertinent to SHM.

Newer devices are characterised by a more compact design, and are therefore lighter in weight (the LIS3LV02DQ weight is 0.2 grams). In this study, mainly aiming to assess the capability of a MEMS-based SHM technique for non-linearly evolving flexible structures, the weight issue was taken aside: we assume the effects of the MEMS-board system on the specimen response to be perfectly known (since it had been measured beforehand), thereby postponing the design and development of wireless sensor networks to be deployed over the plate.

2.2 Monitoring scheme

As said, owing to the capability of the MEMS to detect its own orientation in the three-dimensional space, and specifically with respect to the vertical direction, we used the micro-accelerometer to feel the overall rotation of the board (see Section 2.1).

The basic assumptions behind this monitoring scheme are that the structural component (i.e., the plate) is flexible enough, and that the load actually induces a rotation, i.e., a deflection of the mid-plane. In the next sections, we will show that the above assumptions are easily attained in real-life or standardised situations, independently of the specimen materials.

To track possible changes in the damage state of the structural components, we adopted a time-continuous monitoring protocol. Loading, or displacement-like boundary conditions were quasi-statically varied in time; hence, inertial effects were avoided. This is not strictly necessary for our SHM system to work; instead, dynamically exciting the specimens tested in the validation stage of Section 3 would require to increase the load frequency up to KHz, and an accurate instrumentation of the specimen to track the delamination length would become impossible with the available facilities and sensors.

The monitoring system looks for a variation in the oscillations of acceleration components measured by the MEMS. In forthcoming Section 3, we will show that such variation can be directly linked to the extent of the damaged/cracked area, in accordance with a simplified theoretical description of the test. Moreover, in a parallel investigation (Mariani et al., 2011) we showed that the time-varying data acquired from the MEMS were also in good agreement with finite element simulations of the test.

3 Validation of the proposed method

We first assessed the capability of the offered SHM system to track damage evolution.

To start with a very simple case, we considered a laminate composite specimen subject to a so-called double cantilever beam (DCB) test, see Figure 1. Such test is typically adopted to measure the interlaminar strength and toughness of laminates, as described in Section 3.1. It is worth mentioning that damage is initially represented in this case by a pre-crack, already present inside the specimen at the beginning of testing; because of loading, the crack is opened and damage growth is thereby represented by an advancement of the crack tip. In standard situations, the damage can by effectively and

accurately controlled during the test within a stable regime; hence, numerical and theoretical descriptions of the test turn out to be simple to obtain, see Section 3.3 and (Mariani et al., 2011).

Figure 1 (a) Test set-up and notation (drawing not to scale) (b) Specimen arms bent by the applied load-point displacement (see online version for colours)

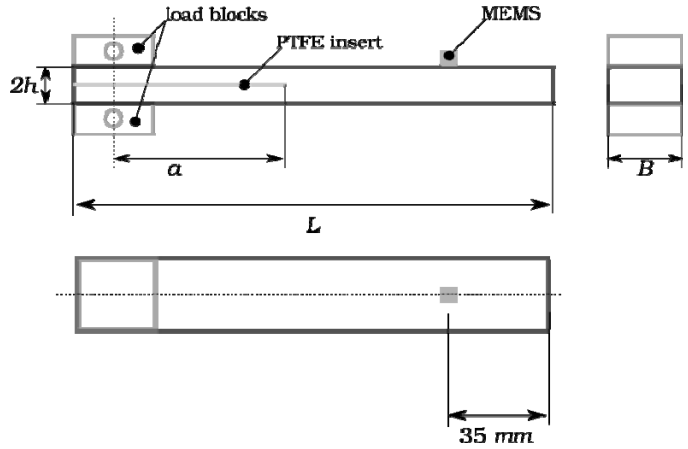

(a)

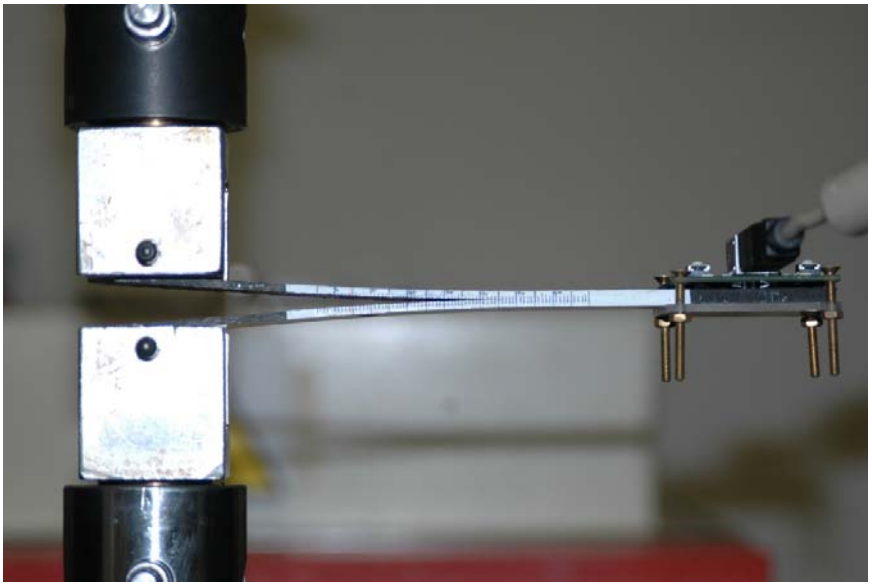

(b)

3.1 Materials and sample preparation

Samples were made starting from Advanced Composites Group MTM-57 unidirectional carbon/epoxy pre-pregs. Nominal fibre volume fraction was 63%. Laminates made of ten pre-preg plies were manually laid up on a tooling plate according to the stacking

sequence $[0°]_{10}$ and vacuum bag cured. The laminate underwent the following curing cycle: rapid heating from ambient temperature to 120°C at 3°C/min, hold for an hour, cooling to 80°C at 3°C/min, hold for half an hour, vacuum release and slow cooling to ambient temperature. During the manual lay-up a 50 μm thick PTFE film was inserted on the mid-plane of the laminate to nucleate an initial edge delamination. The plates thus obtained were cut with a diamond saw and brought to proper dimensions with a milling machine.

A sketch of the specimen, compliant with (ISO, 2001), is shown in Figure 1(a). Aluminium load blocks were glued to the specimen at the delaminated edge, in order to connect it to the testing machine. Nominal dimensions for the samples were h = 1.8 mm, B = 20 mm, length of the PTFE insert A = 60 mm, initial crack length (distance from the load block centre to the end of the PTFE insert) a = 50 mm, L = 200 mm. The accelerometer was placed at 35 mm from edge, at the centreline of the sample. Figure 2 shows a picture of a sample together with the evaluation board and its very simple gripping system, made of a PMMA plate and four screws.

Figure 2 Side and top views of the DCB specimen-MEMS board system (see online version for colours)

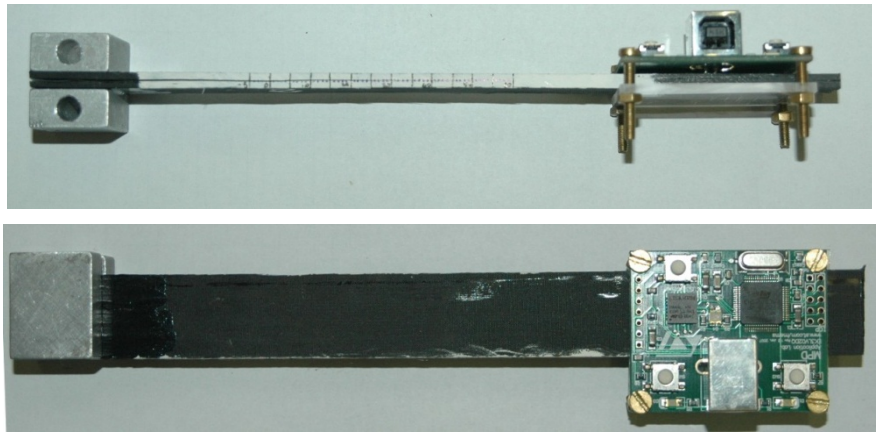

The elastic modulus of the laminate in the fibre direction (namely, in the longitudinal direction) was 90 GPa; the mode I interlaminar fracture toughness was previously determined to be 240 J/m^2 (Salerno et al., 2010).

3.2 Apparatus and test parameters

All of the tests were conducted on an Instron 1185R5800 electro-mechanical testing machine equipped with a 10 kN load cell. The test were performed at 23°C, 50% RH under displacement control. Figure 1(b) shows one specimen while tested, with the two cantilever arms bent by the testing grips.

The displacement history here considered consisted of a ramp to some displacement value u_0, followed by a sinusoidal variation of the displacement around the average value u_0. Oscillation frequency and amplitude were set to f_u = 0.5 Hz and Δu = 2 mm, respectively. Various test phases were run on each sample at increasing u_0 values; within each stage, the average displacement was selected in order to obtain, during the initial

ramp, a crack propagation of about 2 mm or 4 mm, thus allowing studying the response under a cyclic load at varying crack length using a single specimen.

3.3 Sensor placement

Prior to any optimisation studies aimed to define the best position and orientation of the MEMS to monitor damage growth, the adopted geometrical configuration of the test was simply chosen as shown in Figure 2. This way, the sensor was placed in the farthest position away from the initial crack tip to allow monitoring up to an extensive delamination growth, and to ensure measurement of the structural response (and not only of crack growth-induced local dynamics).

The observed acceleration time histories along the longitudinal and vertical axes were directly acquired through the evaluation board.

3.4 Theoretical analysis

Because of the small thickness to crack length $\frac{h}{a}$ ratio, shear deformations of the composite plate (or beam) can be disregarded (Davies and Banzeggagh, 1989). According to Bernoulli-Euler beam bending, the compliance C of the specimen, i.e., the coefficient linking the load-point displacement u to the applied load P, can be written as (see also Figure 1):

$$C = \frac{u}{P} = 8\frac{a^3}{E_l B h^3} \tag{1}$$

where E_l is the effective Young's modulus of the composite in the longitudinal direction. If C is measured during the test at constant crack length, e.g., through unloading paths in the $P - u$ plane, equation (1) can be exploited to determine the current value of a, according to:

$$a = \sqrt[3]{\frac{E_l B h^3}{8} C} \tag{2}$$

The above equations hold true in case of negligible masses added to the specimen. The weight of the MEMS-board system is instead affecting them. Simple equilibrium considerations show that in this case the upper and lower arms of the specimen are not stressed at the same level. In order to still adopt equation (2) to compute the crack length a from the measured compliance C, we therefore accounted for load and displacement fluctuations during one period of the cyclic test. This way, results turn out to be unaffected by the aforementioned weight, and become objective as for the evaluation of a.

To provide a theoretical description of the results of the cyclic tests, we now write the acceleration ü measured by the MEMS as:

$$\ddot{v} = \varphi P \tag{3}$$

where φ is a geometry-dependent coefficient linking ü to the applied load. For ease of analysis, we assume φ to be constant. Accounting for equation (1), and for the time variation of the applied load-point displacement, we then obtain:

$$\ddot{v} = \varphi \frac{u}{C} = \frac{\varphi}{C}\left[u_0 + \Delta u \sin(2\pi f_u t)\right] \tag{4}$$

where u_0 is the aforementioned mean displacement in a cycle; Δu is half its total fluctuation; f_u is the frequency of the driving applied displacement. The magnitude of the Fourier transform of (4) reads:

$$\left|\hat{\ddot{v}}\right| = \frac{\varphi}{C}\left[u_0 \delta(f) + \frac{\Delta u}{2}\delta(f \pm f_u)\right] \tag{5}$$

where $\delta(\cdot)$ stands for the Dirac delta. At $f = f_u$, leaving on the right hand side only the contributions arising from the actual specimen configuration and geometry, it holds:

$$\frac{\left|\hat{\ddot{v}}\right|}{\Delta u} = \frac{\varphi}{2C}\delta(f - f_u) \tag{6}$$

The structure of equation (6) suggests that it is possible to directly correlate the acceleration measurements to crack length (through compliance C) through the intensity of the peak p^M of the Fourier transform at $f = f_u$. Thus $|\hat{\ddot{v}}|(f_u)/\Delta u$, as suggested by this theoretical model, will be adopted in the next section to qualitatively assess the capability of the offered SHM procedure to track the load-induced kinetics of the crack length a.

3.5 Results

In this first experimental campaign, we tested four nominally identical specimens (see Figure 1). To induce damage (delamination) growth, each sample was subject to a series of cyclic tests, featuring a continuously increasing average imposed displacement u_0 and a constant fluctuation Δu = 2 mm. To ensure adaptation of the crack to the imposed loading, each test lasted 100 cycles.

Test results are reported in Figure 3 in terms of measured load P vs imposed load-point displacement u. All the graphs do not start from the origin of the $P - u$ plane because of the weight of MEMS-board; as already described in Section 3.4, the load cell measures the stress induced in the specimen and the board weight too. Orange and blue curves alternatively display the specimen response in subsequent tests under different values of u_0; each stage is characterised by an initial load drop (similar to a pop-in), followed by a stabilised cycle. The overall response of the specimens is always stable under displacement control, and the reducing slope of subsequent cycles in the $P - u$ plane allows computing the value of the crack length at the end of each test (see Section 3.4).

Figure 3 Experimental load P vs displacement u plots, (a) specimen A (b) specimen B (c) specimen C (d) specimen D (see online version for colours)

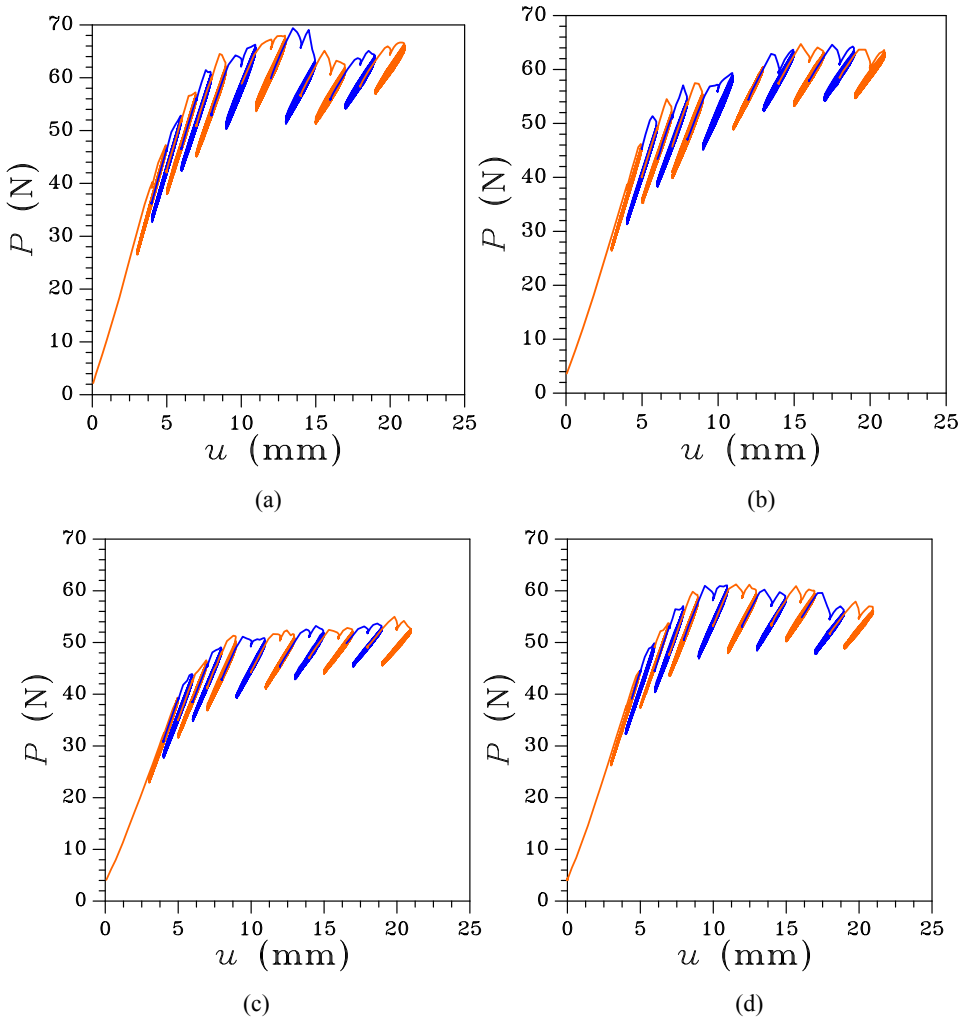

To better understand what happens during each cyclic test starting from u_0, Figure 4 shows the time evolution of load P relevant to specimen A and load phase 8 [see also Figure 3(a)]. The inset helps to display the typical evolution of P at the beginning of the test. Because of the increased u_0 (with respect to the previous load phase), the specimen is not able to sustain the induced tractions ahead of the crack tip: delamination therefore grows and P suffers a drop (see the horn-like couple of peaks in the inset, around t = 15 s). After this initial delamination stage, the load gets almost stabilised, even if maxima and minima in the subsequent evolution continuously decrease to testify a stable delamination growth.

Figure 4 Specimen A, load phase 8: experimental load P vs time t-plot (see online version for colours)

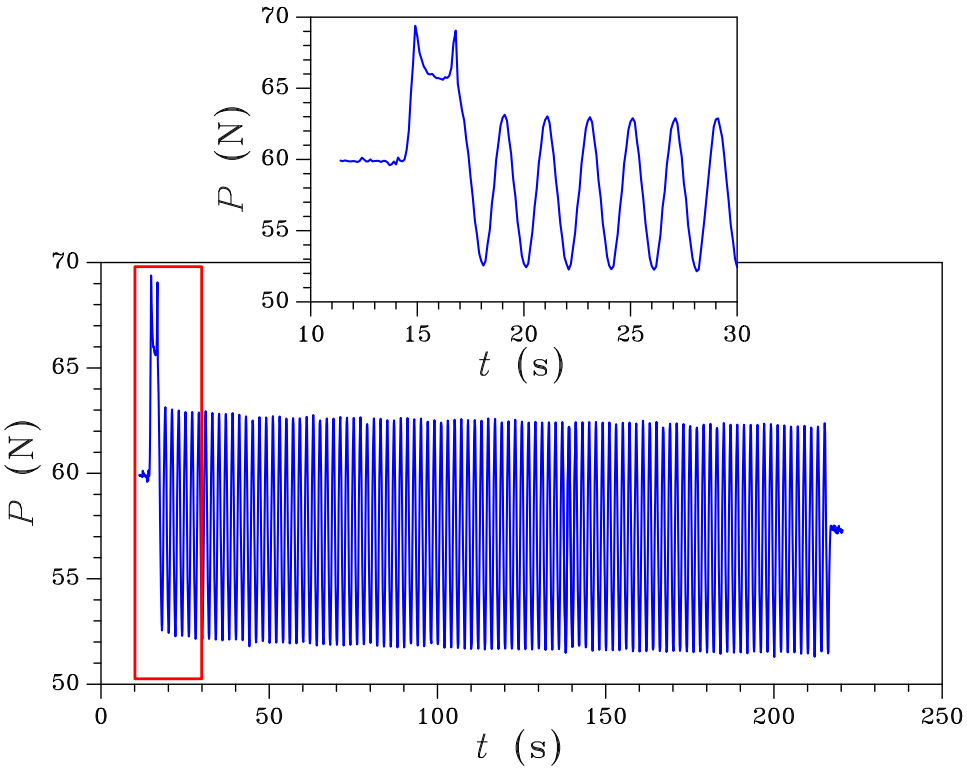

Moving now to the measurements obtained through the MEMS, Figure 5 reports a comparison between the slowly (sinusoidally) fluctuating load P and the acceleration components a_x and a_z (respectively, longitudinal and vertical ones in the initial unstressed state); because of signals coming from two different acquisition systems, load and accelerations are here shifted in time. Despite the much higher noise level, as compared to the measured load, acceleration components show main fluctuations at the test frequency of 0.5 Hz.

To get rid of all the spurious higher frequency oscillations, we move to the frequency domain, and adopt the theoretical description of Section 3.4 to handle the peak values p^M of the Fourier transform of the signals at 0.5 Hz. Figure 6 shows the results of the four test series, in terms of normalized frequency peak $\frac{p^M}{u_0}$ as a function of the relevant crack length a. Besides some scattering induced by material properties fluctuation along the debonding interlaminar surface (see also Mariani et al., 2013b), all the plots show a decay in good agreement with the theoretical $\frac{1}{C}$ one.

Figure 5 Specimen A, load phase 1: experimental (a) load P *vs* time t, and (b) a_x, a_z components of the acceleration *vs* time t plots (see online version for colours)

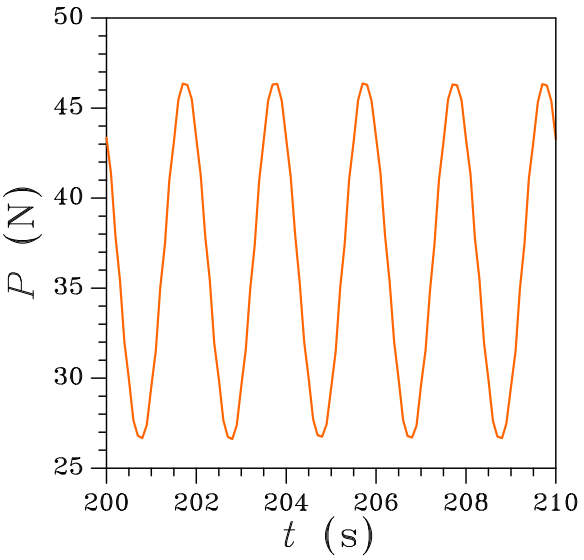

(a)

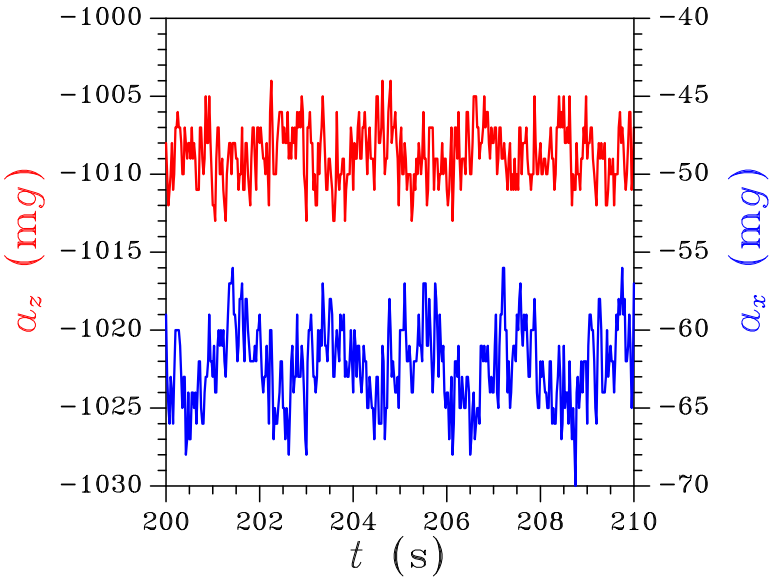

(b)

Figure 6 Experimental normalised frequency peak $\frac{p^M}{\Delta u}$ *vs* crack length *a* plots, (a) specimen A (b) specimen B (c) specimen C (d) specimen D (see online version for colours)

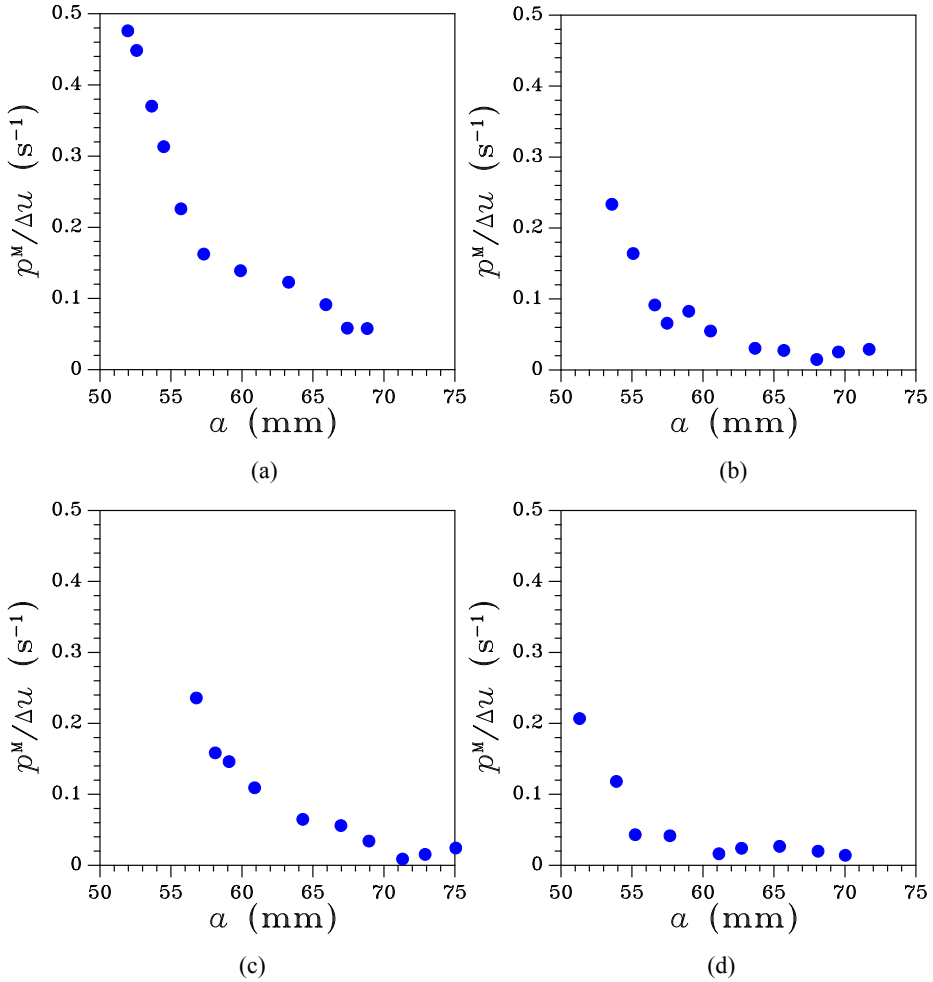

4 Optimal sensor placement

We now address a second main issue in the development of an efficient SHM system: the optimal placement of the sensors to accurately track a change in the damage state. To slightly simplify the analysis, we consider here an isotropic plate wherein damage is represented by a zone of reduced bending stiffness; this may be linked with the presence of an interlaminar crack, like that considered in Section 3, or with a reduced thickness of the plate.

With a slight abuse in terminology, we claim to adopt here a topology optimisation approach. Actually, since we are not optimising the topology of the load-bearing structure (i.e., of the plate) but instead the topology of the added sensing system, this cannot be classified as a topology optimisation problem. At any rate, we approached the problem as typically done in topology optimisation.

4.1 Optimisation approach

What is sought here is the optimal placement of a fixed set of sensors, so as the sensitivity of the SHM system to the damage gets maximised. This problem may be tackled through an optimisation engine that searches for the best distribution of measurables, and may be conveniently solved taking advantage of mathematical programming tools.

4.1.1 General form of an optimisation problem

Following (Duysinx et al., 2009), we formulate a quite general optimisation problem as follows:

$$\begin{cases} \min_x \psi_0 \\ s.t. \\ g_j(x) \le \overline{g_j} \qquad j = 1,\dots,m \\ \breve{x}_l \le x_i \le \overline{x}_l \qquad i = 1,\dots n \end{cases} \tag{7}$$

The function ψ_0 is the objective function of the problem, i.e., a performance index that has to be minimised in order to achieve the best design, in our case the best sensor placement. The set of m constraint functions g_j enforces suitable restrictions that the design has to fulfill in order to be feasible. The n variables x_i are the unknowns of the problem, i.e., the parameters which can be modified to improve the design; they are subject to some restrictions that depend on physical or mathematical reasons, and are usually defined as side constraints.

The direct solution of the primary optimisation problem (7) is generally a very difficult task, due to the computational burden that is tied to the evaluation of the objective function and to the relevant sensitivity analysis of the problem. This becomes a crucial issue in structural optimisation problems, where ψ_0 may be a highly non-linear and implicit function of the design variables x_i (see e.g., Bendsøe and Sigmund, 2003). To overcome this, Schmidt and Fleury (1980) firstly proposed to replace the primary optimisation problem with a sequence of explicit, approximate sub-problems. Hence, it is possible to build sub-problems having a simple algebraic structure like:

$$\begin{cases} \min_x \widetilde{\psi_0} \\ s.t. \\ \widetilde{g_j}(x) \le \overline{g_j} \qquad j = 1,\dots,m \\ \breve{x}_l \le x_i \le \overline{x}_l \qquad i = 1,\dots n \end{cases} \tag{8}$$

where $\widetilde{\psi_0}$ and $\widetilde{g_j}$ may be seen as a sort of Taylor series expansion of the objective function ψ_0 and constraint functions g_j around the current design point x^k. The sub-problems arising in equation (8) can be efficiently solved with mathematical programming algorithms, like the so-called dual method (Fleury, 1979) with the CONLIN minimiser, also exploited in the method of moving asymptotes, MMA (Svanberg, 1987). Since MMA will be used extensively in the following numerical simulations, some further details of the method are presented next.

4.1.2 The method of moving asymptotes

In order to exploit efficiently dual methods, two features of the sub-problems in equation (8) should be pursued, i.e., convexity and separability. The convexity of the approximation ensures that the solution of the dual problem is the same solution of the original problem. The separability allows deriving an uncoupled system of equations between the primal variables and the dual unknowns, meaning that the problem can be solved independently for each primal variable; this is an essential feature to reduce the computational effort.

MMA provides the above features adopting a convex linearisation scheme that may be regarded as a first order Taylor series expansion in terms of the intermediate variables $1/(U_i - x_i)$ and $1/(x_i - L_i)$. U_i and L_i are the so-called vertical asymptotes values for which, around the current design point $\boldsymbol{x}^k$, one has $L_i^k < x_i^k < U_i^k$. After normalisation, the MMA approximation of equation (7) may be written as:

$$\begin{cases} \min_x \sum_{i=1}^{n} \left(\dfrac{r_{i0}}{U_i - x_i} + \dfrac{s_{i0}}{x_i - L_i} \right) \\ s.t. \\ \quad \sum_{i=1}^{n} \left(\dfrac{r_{ij}}{U_i - x_i} + \dfrac{s_{ij}}{x_i - L_i} \right) \le d_j \qquad j = 1, \ldots, m \\ \quad \underline{x}_i \le x_i \le \overline{x}_i \quad i = 1, \ldots, n. \end{cases} \tag{9}$$

The above objective function calls for the computation of the values r_{i0} and s_{i0} as:

$$r_{i0} = \max\left(0, \left(U_i - x_i^k\right)^2 \frac{\partial \psi_0}{\partial x_i}\right) s_{i0} = \max\left(0, -\left(x_i^k - L_i\right)^2 \frac{\partial \psi_0}{\partial x_i}\right) \tag{10}$$

while each one of the m constraints is written in terms of an approximated right-hand side along with analogous terms of the type:

$$r_{ij} = \max\left(0, \left(U_i - x_i^k\right)^2 \frac{\partial g_j}{\partial x_i}\right) s_{ij} = \max\left(0, -\left(x_i^k - L_i\right)^2 \frac{\partial g_j}{\partial x_i}\right) \tag{11}$$

Once the approximated form of the constrained minimisation setting has been defined, one may straightforwardly derive the Lagrange function associated to the problem,

weighting each constraint with a relevant multiplier γ_j. This transforms the optimisation into an unconstrained problem with a new objective function that depends on both primal x_i and dual γ_j design variables. Because of the separability property, the n-dimensional problem can be split into n one-dimensional problems relative to each variable x_i. The Karush-Kuhn-Tucker conditions require stationarity of the Lagrange function with respect to x as a necessary conditions of optimality for constrained statements. The solution of this problem can be therefore solved explicitly for each variable, to give rise to the primal-dual relations.

According to the above scheme, the original primal minimisation problem becomes a dual maximisation setting, that is easily tackled by MMA. As the number of dual variables is often smaller than the number of primal variables, the dimensionality of the dual optimisation problem is expected to be smaller than the original one. MMA thus looks ideally tailored to work with large set of unknowns, as in the optimal placement of sensors problem.

4.1.3 A formulation for the optimal spatial distribution of sensors

We now move to the optimal placement of an assigned set of sensors over the structure to be monitored. This problem may be framed within a special class of structural optimisation problems, whose unknown is the topology, intended as the spatial distribution (see e.g., Bendsøe and Kikuchi, 1988; Bendsøe and Sigmund, 2003). The discrete form of such formulation usually resorts to the adoption of an underlying grid of finite elements.

We address the case of a homogeneous plate, subject to fixed external forces (e.g., assigned loads or gravity). One may easily discretise the domain with finite elements, and compute the solution in terms of displacements and rotations. If the undamaged structure is analysed, it is possible to define a vector of element-wise constant reference displacements $\hat{u}_i$. If the same plate is affected by a local damage, whose position is known, one may define a vector of current displacements u_i. The optimal placement of sensors to detect the damage may be found by looking for the elements where the difference $\Delta_i = (u_i - \hat{u}_i)^2$ between the two aforementioned solutions is maximised. This may be straighforwardly accomplished framing the problem within the setting of equation (7). According to the conventional problem of topology optimisation, one may define a discrete density field x_i, continuous in the range $0 \le x_i \le 1$, to account for the presence or absence of the sensor on the i^{th} element of the mesh.

The problem of distributing an assigned number $\bar{N}$ of sensors on the structure, to maximise the sensitivity of the SHM system, may be therefore written as:

$$\begin{cases} \max_x \sum_{i=1}^{n} x_i^p \left(u_i - \hat{u}_i\right)^2 \\ s.t. \\ \quad \sum_{i=1}^{n} x_i \le \bar{N} \\ \quad 0 \le x_i \le 1 \quad i = 1,...n \end{cases} \tag{12}$$

In full analogy with penalisation approaches, used to achieve pure 0–1 distributions, a stronger penalisation of the intermediate density may be achieved tuning the penalisation exponent p.

It must be remarked that the evaluation of the objective function in equation (12.1) requires two finite element analyses of the undamaged and damaged plates. The minimiser then calls for straightforward manipulations of the penalisation terms in x_i, to update the objective function and its gradient at each iteration.

4.1.4 Extension to multiple damage location

A more interesting application of the proposed procedure consists in the definition of the optimal sensor layout in the case of a multiplicity of damaged zones. One has therefore to define a suitable objective function which takes into account several damage cases. For each location of the damage, one may compute a set of moduli $\Delta_{ki} = (u_{ki} - \hat{u}_i)^2$, u_{ki} being the displacements measured with damage located in the k^{th} element. The general optimisation setting, taking into account S damage cases, then reads:

$$\begin{cases} \max_x \sum_{k=1}^{s} \left[\sum_{i=1}^{n} x_i^p \left(u_{ki} - \hat{u}_i \right)^2 \right] \\ s.t. \\ \qquad \sum_{i=1}^{n} x_i \le \bar{N} \\ \qquad 0 \le x_i \le 1 \quad i = 1,...n \end{cases} \tag{13}$$

which maximises the sensitivity of the monitoring system to the amplitude of the measured displacements or rotations. This optimisation setting mainly predicts a placement of sensors where they read the maximum variation in the structural response, independently of the source.

To overcome this problem, one may reformulate the objective function weighting the k-th contribution with the maximum Δ_{ki} recorded on the mesh. This relieves the differences in terms of maximum amplitudes among the damage cases, thus asking for an optimal distribution that is more oriented to the detection of damage. The relevant formulation reads:

$$\begin{cases} \max_x \sum_{k=1}^{s} \left[\dfrac{\sum_{i=1}^{n} x_i^p \left(u_{ki} - \hat{u}_i \right)^2}{\max_i x_i^p \left(u_{ki} - \hat{u}_i \right)^2} \right] \\ s.t. \\ \qquad \sum_{i=1}^{n} x_i \le \bar{N} \\ \qquad 0 \le x_i \le 1 \quad i = 1,...n \end{cases} \tag{14}$$

4.2 Results

As already anticipated, simulations in this section are referred to a square, homogeneous and isotropic thin plate, featuring a length to thickness ratio $\frac{L}{h} = 1,000$, see Figure 7. Undamaged (reference) and damaged plate responses were obtained by considering a material featuring a (say, dimensionless) Young's modulus E = 10.92 and a Poisson's

ratio $v = 0.3$ (see also, Zienkiewicz and Taylor, 2000). The plate is simply supported over all its edges, and is subjected to a constant distributed load perpendicular to the mid-plane.

As shown in Figure 7, five different locations of damage were considered; in each case, the damage consists in a reduction of 50% of the local bending stiffness of the plate. These five locations were selected to assess the effects of damage position on the optimal layout of the sensors.

Restricting our analyses to the small strain regime, the plate was discretised with 4-node, shear deformable mixed finite plate elements (Auricchio and Taylor, 1994), which allow to attain the exact thin limit solution even if the kinematics of moderately thick plates is adopted. Such elements are available with the FEAP code (Taylor, 2003), here adopted to feed the topology optimiser. The plate was discretised with a structured mesh, subdividing each edge into 33 elements. Such discretisation allows to achieve convergence toward the theoretical values of central deflection and bending moments, and also accounts for the size of the evaluation board shown in Figure 2. Hence, each element is here considered to be the placement and extension of the damage, and also a position where a sensor can be placed.

Figure 7 Square plate: notation and position of the damaged areas relevant to cases #1–#5 (see online version for colours)

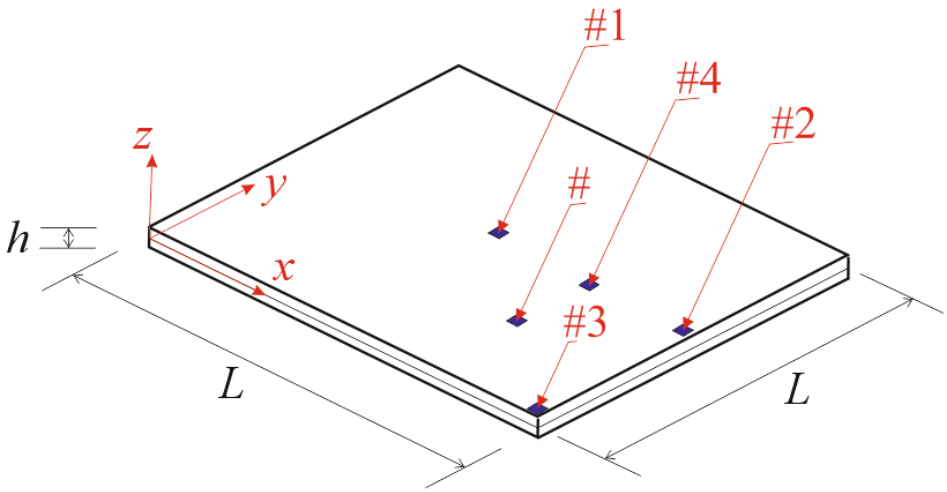

Results relevant to the undamaged case are reported in Figure 8 in terms of (see Figure 7 as for the notation): rotations θ_x and θ_y around the x and y axes, respectively; norm of the rotation $\theta = \sqrt{\theta_x^2 + \theta_y^2}$, here adopted to symmetrise the solution; deflection w_z. As reported in Section 4.1, the topology optimisation tool handles results according to an element-wise data structure; this explains why the contour plots in Figure 8 and subsequent ones were not smoothed.

Figure 8 Square plate: undamaged solution in terms of (a) θ_x (b) θ_y (c) $\theta = \sqrt{\theta_x^2 + \theta_y^2}$ and (d) w_z (see online version for colours)

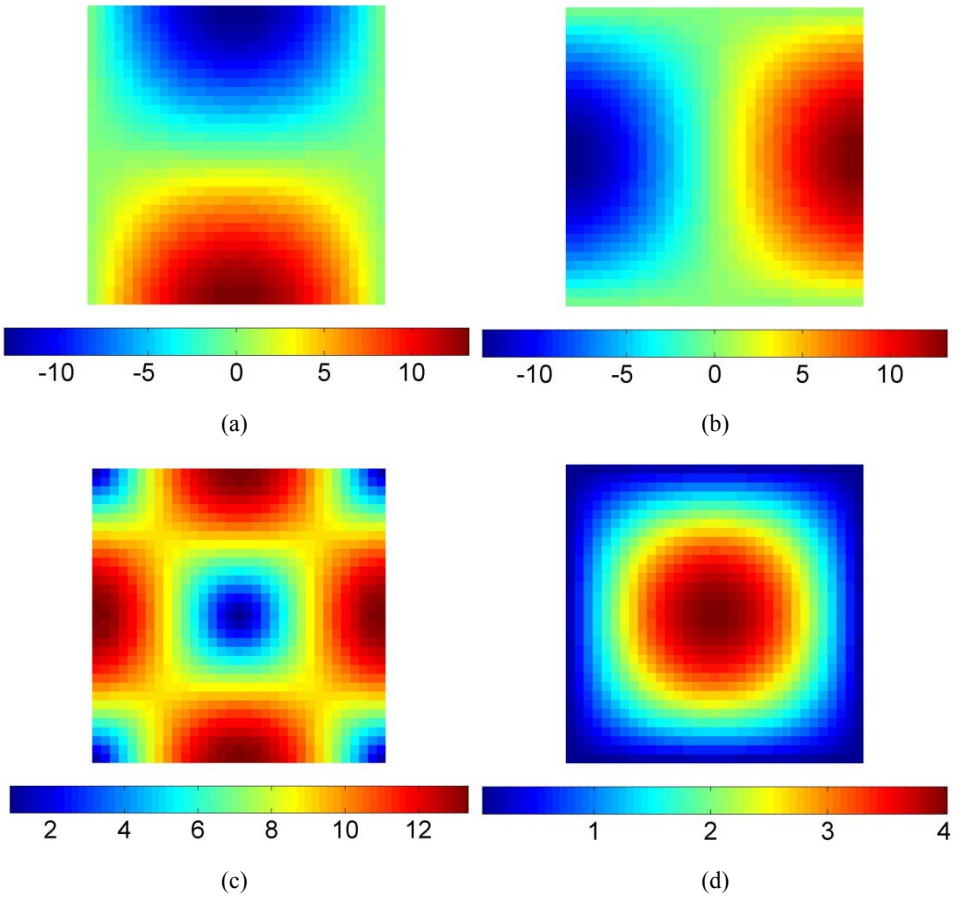

To understand the effects of damage and damage location on the plate response, Figures 9–11 report the variations in the solution (once again, in terms of θ_x, θ_y, θ and w_z) with respect to the undamaged case for the three main damage cases #1, #2 and #3, respectively; similar results were obtained for damage cases #4 and #5, and are not reported here for brevity. To comparatively assess the outcomes, all these contour plots have been normalised to get confined within the [–1 1] interval; red (blue) spots are thus characterised by a solution approaching +1(–1), whereas the green area displays almost no variations, and so zero sensitivity to the presence of damage. As expected, the sensitivity is higher close to the damage location, and the spreading of the area of higher sensitivity depends on the observed variable. The different locations of damage allow to also understand how damage interacts with the boundary conditions along the plate edges; for instance, since deflection w_z is zero along the supported sides, the region featuring positive sensitivity moves toward the centre of the plate, where the displacement is not constrained [see Figure 10(d)]. In all these figures, the sensitivity of w_z to the damage is shown only for comparison, since in Section 2 we already stated that

MEMS accelerometers were adopted to monitor variations of local rotations. Moreover, using a three-axis accelerometer allows to monitor rotation about the two orthogonal in-plane axes; hence, dealing with the magnitude θ of the rotation vector helps in increasing the sensitivity of measurables to the damage, and to simultaneously increase the area of positive sensitivity.

Figure 9 Square plate, damage case #1: variation with respect to the undamaged solution in terms of (a) θ_x (b) θ_y (c) $\theta = \sqrt{\theta_x^2 + \theta_y^2}$ (d) w_z (see online version for colours)

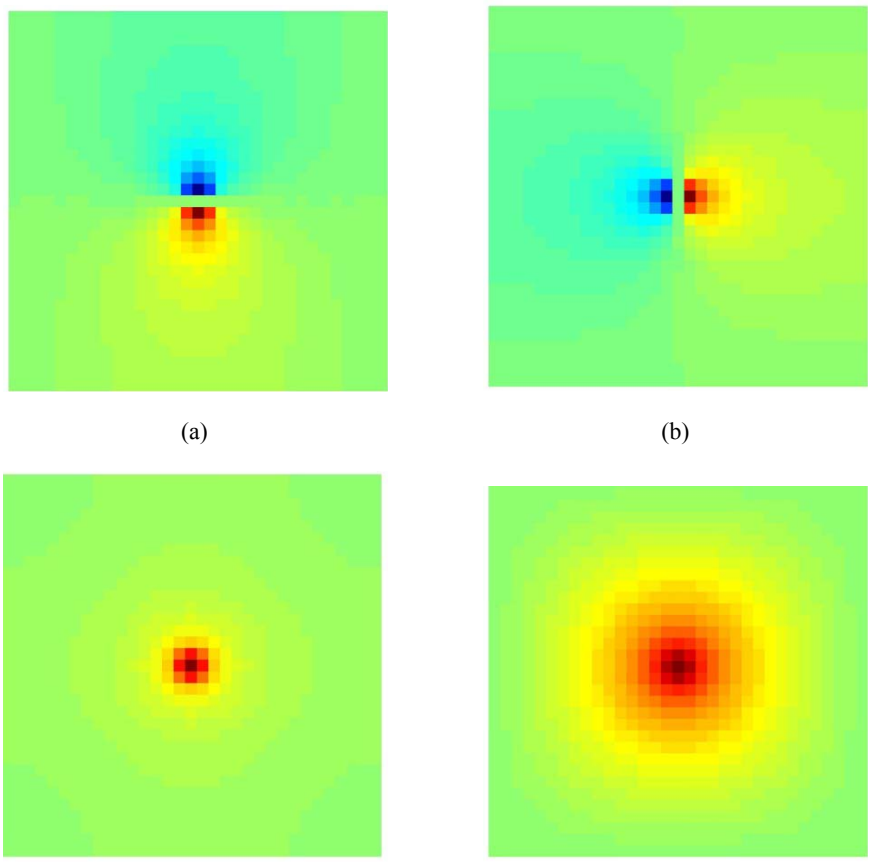

(a) (b)

(c) (d)

Figure 10 Square plate, damage case #2: variation with respect to the undamaged solution in terms of (a) θ_x (b) θ_y (c) $\theta = \sqrt{\theta_x^2 + \theta_y^2}$ (d) w_z (see online version for colours)

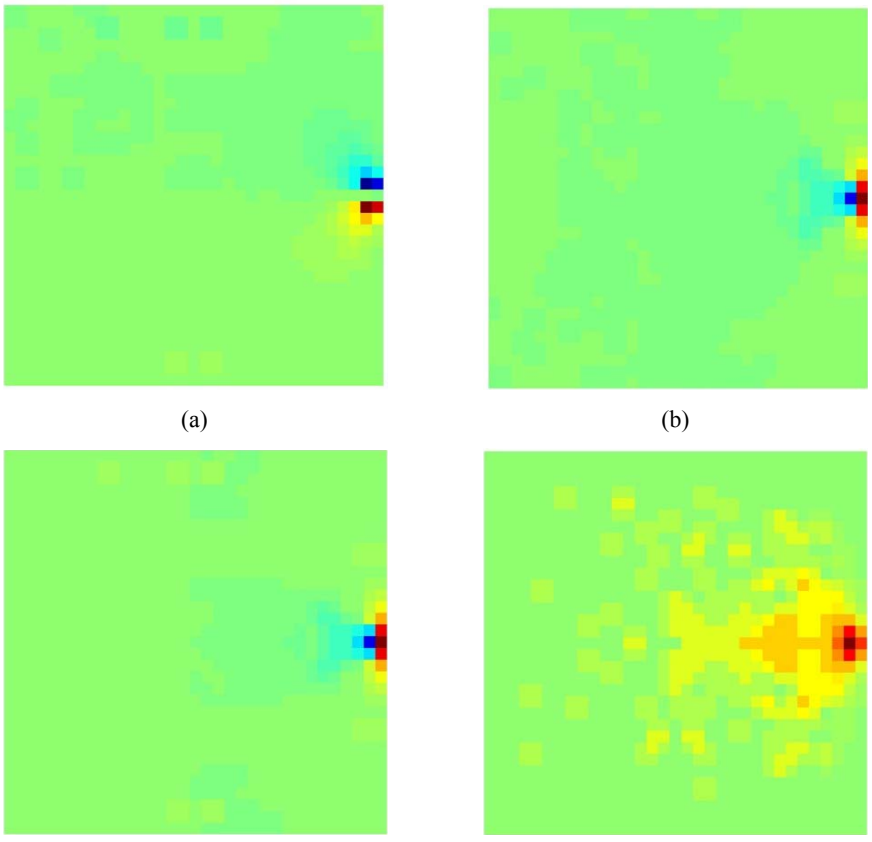

To display results relevant to the optimal placement of sensors, we considered first the case $\bar{N} = 2$ (see Section 4.1.3). This choice was basically routed by the results commented here above: since sensitivity is maximum at, or close to damage location, $\bar{N} = 2$ allows us to check where the algorithm places an additional sensor (besides the one above the damaged area) to monitor the global health of the plate. Once again, we considered θ_x, θ_y, θ and w_z as possible measurables, even though w_z has to be considered only as a benchmarking example for our SHM approach. It is worth mentioning that the topology optimisation algorithm does not necessarily deploy sensors according to a 0–1 distribution; because of symmetries in the solutions, it happens that grey levels refer to regions (elements) featuring the same sensitivity, all summing up to give $\bar{N} = 2$.

Figure 11 Square plate, damage case #3: variation with respect to the undamaged solution in terms of (a) θ_x (b) θ_y (c) $\theta = \sqrt{\theta_x^2 + \theta_y^2}$ (d) w_z (see online version for colours)

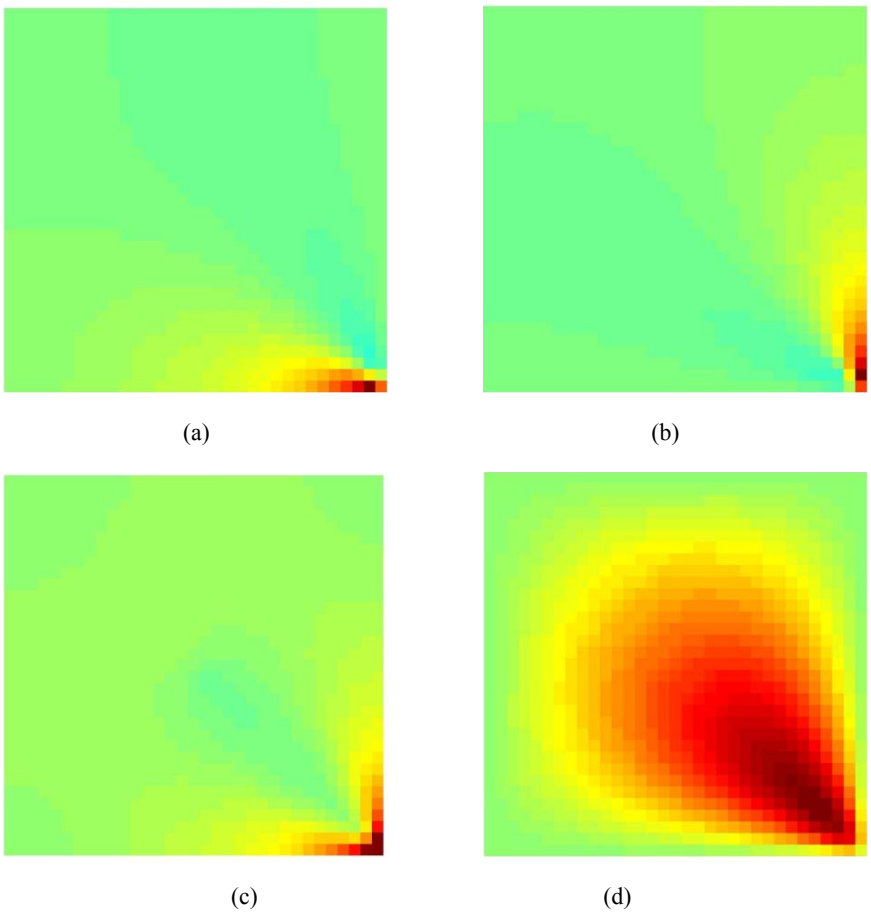

Figures 12–14 show the obtained optimal placements to sense the three main damage locations considered before. Remarkably, sensors are always placed over the damage or over neighbouring elements, except when the boundary conditions lead to zero deflections or rotations, i.e., to zero sensitivity to damage; in such cases, sensors are moved toward the center of the plate, according to the previously shown sensitivity maps. Handling θ, instead of θ_x or θ_y, allows to symmetrise the sensor placement with respect to the damage, which is quite expected because of the symmetry displayed by the geometry of the plate and by the boundary and loading conditions.

Figure 12 Square plate, damage case #1: optimal deployment of two sensors to monitor variations of (a) θ_x (b) θ_y (c) $\theta = \sqrt{\theta_x^2 + \theta_y^2}$ (d) w_z

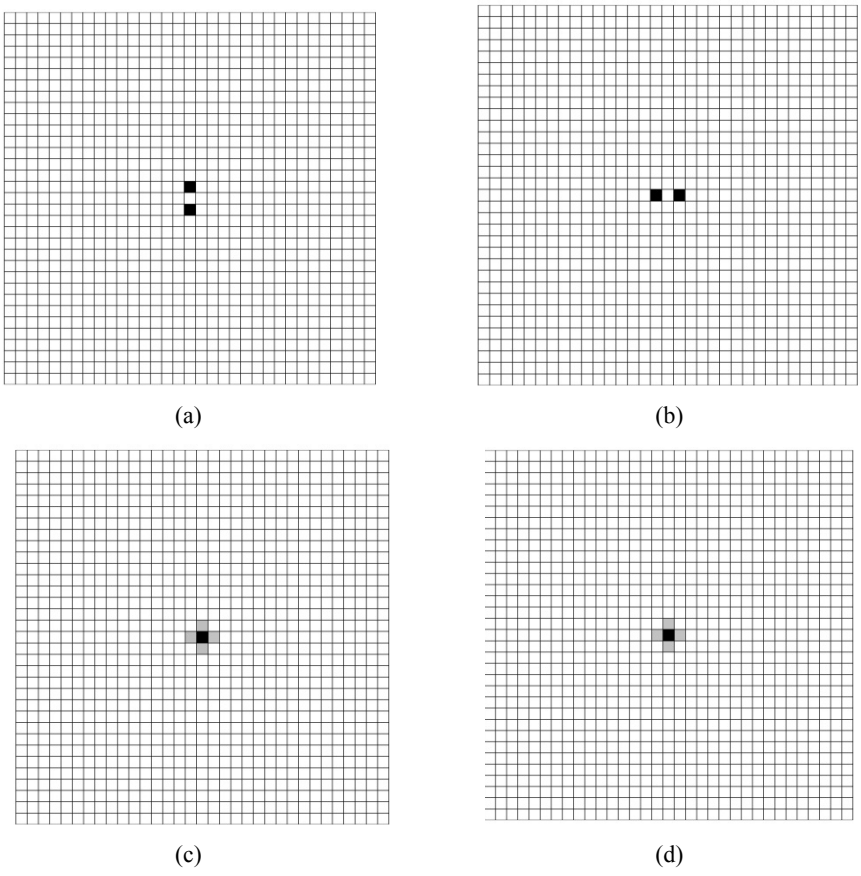

(a) (b)

(c) (d)

Figure 13 Square plate, damage case #2: optimal deployment of two sensors to monitor variations of (a) θ_x (b) θ_y (c) $\theta = \sqrt{\theta_x^2 + \theta_y^2}$ (d) w_z

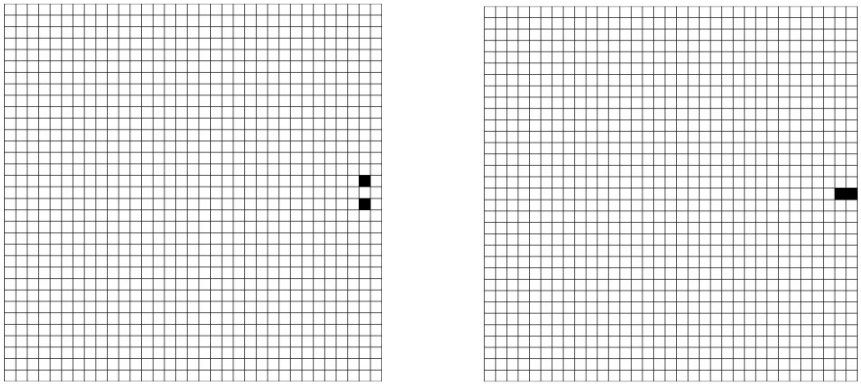

(a) (b)

Figure 13 Square plate, damage case #2: optimal deployment of two sensors to monitor variations of (a) θ_x (b) θ_y (c) $\theta = \sqrt{\theta_x^2 + \theta_y^2}$ (d) w_z (continued)

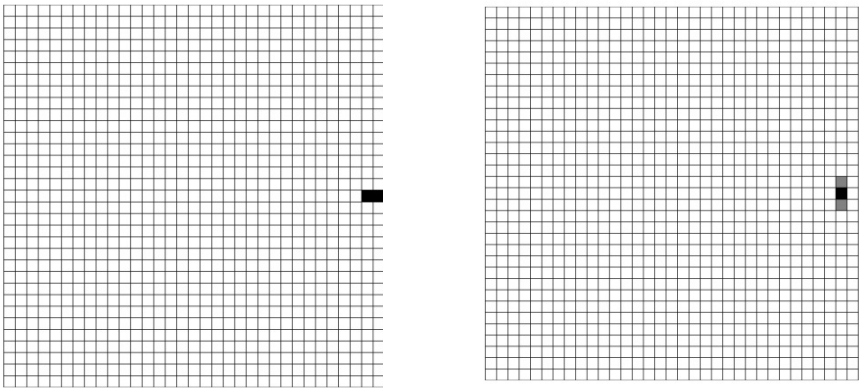

(c) (d)

Figure 14 Square plate, damage case #3: optimal deployment of two sensors to monitor variations of (a) θ_x (b) θ_y (c) $\theta = \sqrt{\theta_x^2 + \theta_y^2}$ (d) w_z

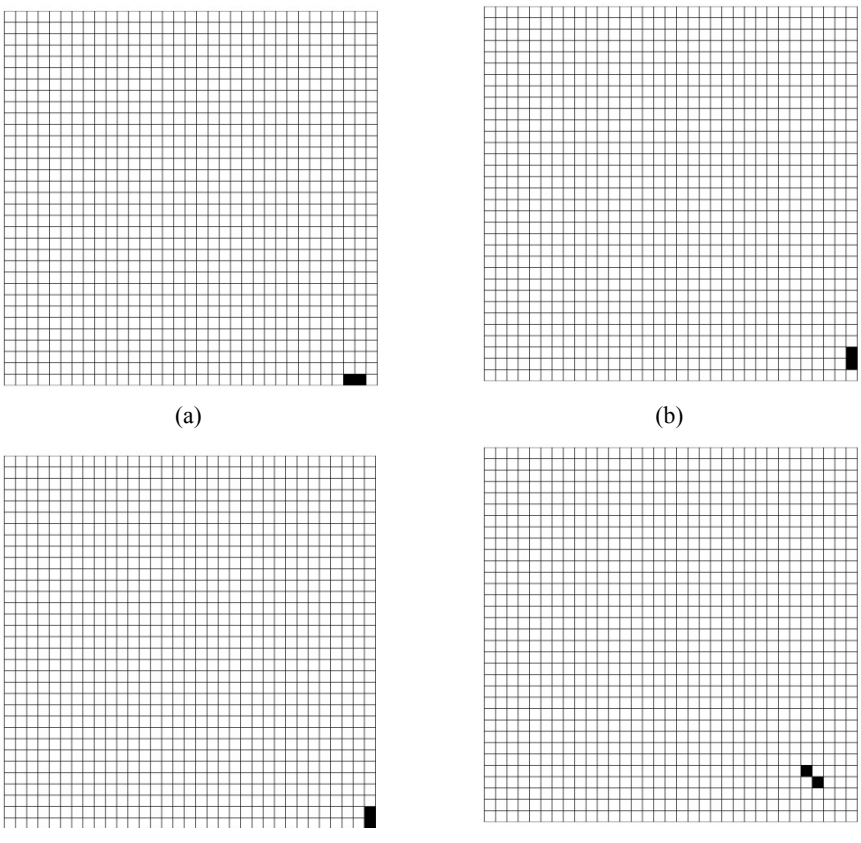

(a) (b)

(c) (d)

To further understand how sensors should be placed, Figures 15 and 16 report the optimal topology for cases #1 and #3, when $\bar{N}=1$ and $\bar{N}=10$. It can be seen that, independently of $\bar{N}$, sensors are always deployed around, or close to the damage source, so as to enhance the sensitivity to the damage itself.

Figure 15 Square plate, damage case #1: optimal deployment of $\bar{N}$ sensors to monitor variations of $\theta=\sqrt{\theta_x^2+\theta_y^2}$ (a) $\bar{N}=1$ (b) $\bar{N}=10$

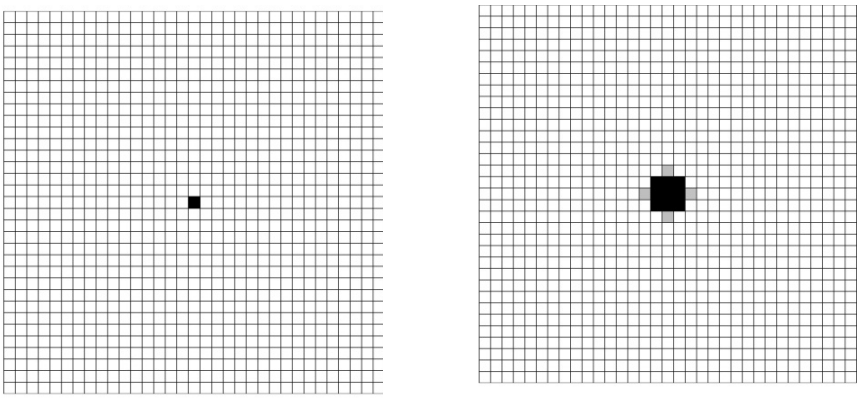

(a) (b)

Figure 16 Square plate, damage case #3: optimal deployment of $\bar{N}$ sensors to monitor variations of $\theta=\sqrt{\theta_x^2+\theta_y^2}$ (a) $\bar{N}=1$ (b) $\bar{N}=10$

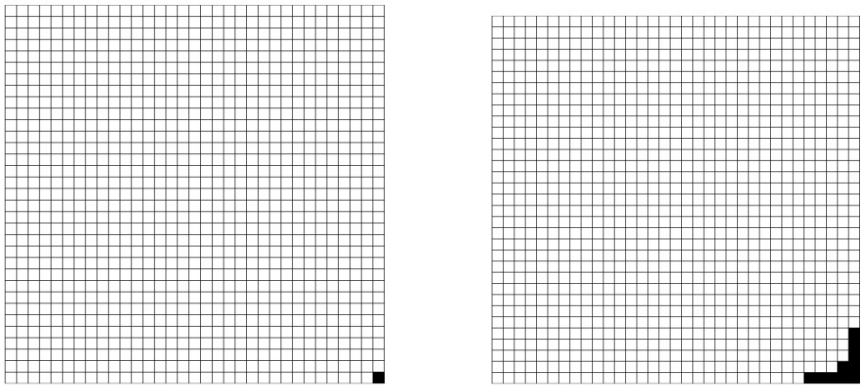

(a) (b)

Finally, results are presented in Figures 17 and 18 when variations of θ are monitored, at varying $\bar{N}$ and handling together all the five damage cases, hence for damage placed anywhere inside the selected locations. The two series of results are respectively relevant to the optimal formulations (13) and (14): in the former case (Figure 17) the sensivities are handled as are, and the algorithm therefore placed sensors where the total variation of θ is higher, i.e., at the centre of the plate first and then (when $\bar{N}$ is increased) around the

other locations; in the latter case (Figure 18) the sensitivity to damage is instead maximised, and sensors were therefore deployed with almost the same pattern of the assumed damage distribution.

Figure 17 Square plate, all damage cases handled together: optimal deployment of sensors to monitor variations of $\theta = \sqrt{\theta_x^2 + \theta_y^2}$, (a) $\bar{N} = 1$ (b) $\bar{N} = 2$ (c) $\bar{N} = 10$ (d) $\bar{N} = 50$

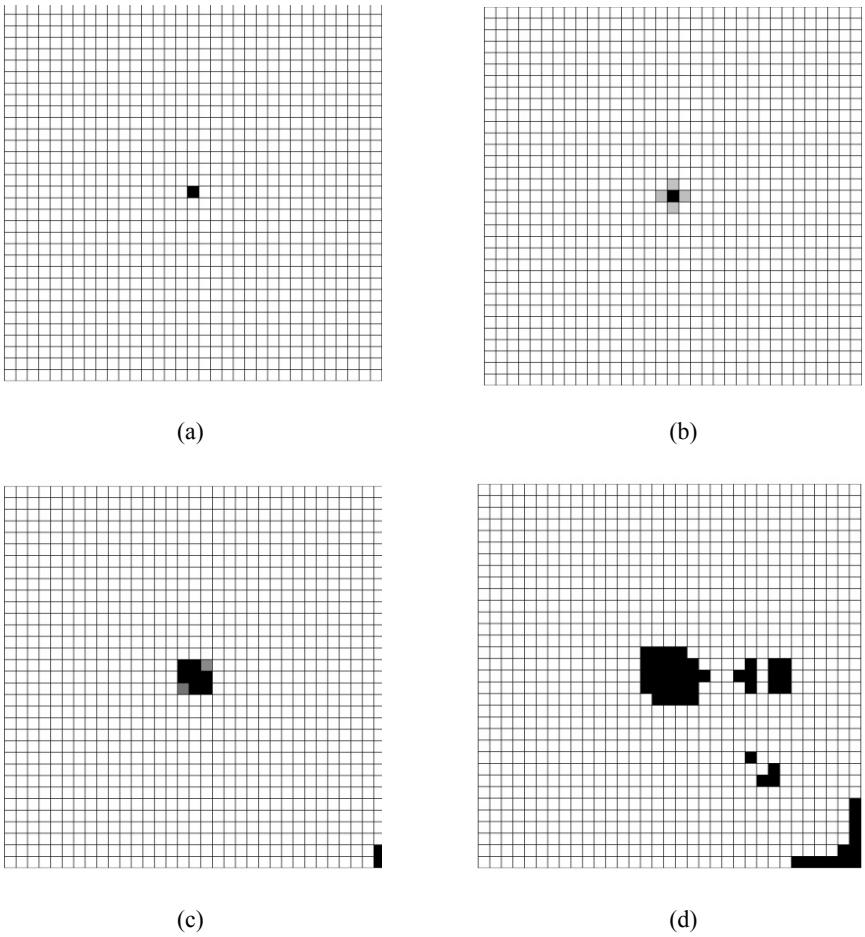

(a) (b)

(c) (d)

Figure 18 Square plate, all damage cases handled together: optimal deployment of sensors to monitor non-dimensional variations of $\theta = \sqrt{\theta_x^2 + \theta_y^2}$, (a) $\bar{N} = 1$ (b) $\bar{N} = 2$ (c) $\bar{N} = 10$ (d) $\bar{N} = 50$

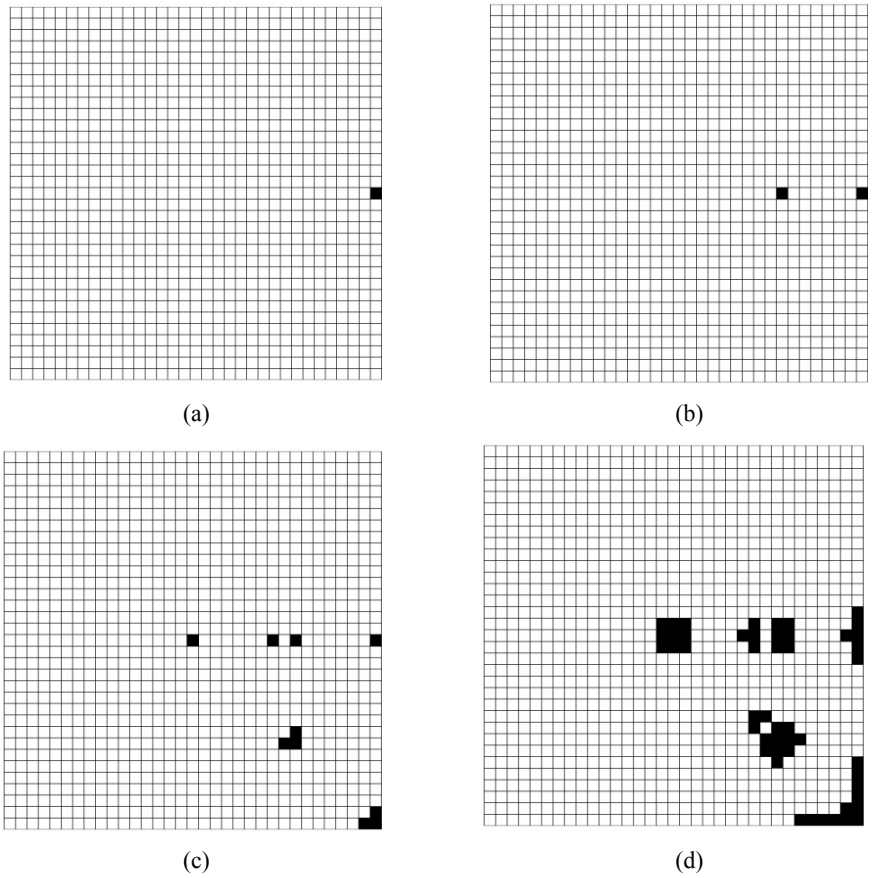

(a) (b)

(c) (d)

Additional results, accounting for damage possibly located anywhere in the plate, hence not only inside the five areas here considered, were already presented and discussed in (Bruggi and Mariani, 2013; Mariani et al., 2013a). It is worth noting that such results, in terms of deployment patterns, completely hide the actual location of damage, since the SHM system is asked to have maximum sensitivity independently of the damage location itself. As already mentioned in the introduction, this general strategy therefore requires a filtering stage to eventually locate the actual position of the damaged area over the mid-plane of the plate.

5 Concluding remarks

In this work, we have presented and discussed a MEMS-based health monitoring system for flexible plates. To first assess the capability of the proposed methodology, we tested crack-containing composite specimens in a double cantilever beam configuration, and adopted a slowly varying opening displacement (or force) to induce a monotonically increasing damage (delamination) length. Using low-cost commercial off-the-shelf MEMS accelerometers, rigidly linked to the specimens, we obtained a crack length sensing system.

We have then approached the problem of optimal placement of the sensors. We proposed a topology optimisation-like approach to deploy the MEMS so as to maximise the sensitivity to defects. We exploited this procedure to study a square, homogeneous and thin plate, simply supported along its edges and featuring localised damaged areas of known extent and location. We numerically proved that the proposed scheme optimally places the sensors close to the damaged areas, i.e., in the regions where the sensitivity to the presence and possible growth of damage is higher.

Next steps of the present study will be:

1 a check of the repeatability of the results, to assess the robustness of the offered MEMS-based monitoring system

2 the development of a (possibly wireless and self-powered) electronics, able to simultaneously manage signals coming from several sensors deployed over real-life structures.

References

Abrate, S. (1998) *Impact on Composite Structures*, Cambridge University Press.

Auricchio, F. and Taylor, R.L. (1994) 'A shear deformable plate element with an exact thin limit', *Computer Methods in Applied Mechanics and Engineering*, Vol. 118, Nos. 3–4, pp.393–412.

Bendsøe, M.P. and Kikuchi, N. (1988) 'Generating optimal topologies in structural design using a homogenization method', *Computer Methods in Applied Mechanics and Engineering*, Vol. 71, No. 2, pp.197–224.

Bendsøe, M.P. and Sigmund, O. (2003) *Topology Optimization – Theory, Methods and Applications*, Springer, EUA, New York.

Bruggi, M. and Mariani, S. (2013) 'Optimization of sensor placement to detect damage in flexible plates', *Engineering Optimization*, Vol. 45, No. 6, pp.659–676.

Corigliano, A. and Mariani, S. (2004) 'Parameter identification in explicit structural dynamics: performance of the extended Kalman filter', *Computer Methods in Applied Mechanics and Engineering*, Vol. 193, Nos. 36–38, pp.3807–3835.

Davies, P. and Banzeggagh, M.L. (1989) 'Interlaminar mode-I fracture testing', *Chapter 3 of Application of Fracture Mechanics to Composite Materials*, K. Friedrich, K. (Ed.), pp.81–112, Elsevier Science Publishers B.V, Amsterdam, The Netherlands.

Duysinx, P., Bruyneel, M. and Fleury, C. (2009) *Solution of Large Scale Optimization Problem With Sequential Convex Programming*, Lecture notes for the Advanced course in Topology Optimization delivered by the Danish Center For Applied Mathematics and Mechanics.

Fleury, C. (1979) 'Structural weight optimization by dual methods of convex programming', *International Journal for Numerical Methods in Engineering*, Vol. 14, No. 12, pp.1761–1783.

Ghisi, A., Fachin, F., Mariani, S. and Zerbini, S. (2009a) 'Multi-scale analysis of polysilicon MEMS sensors subject to accidental drops: effect of packaging', *Microelectronics Reliability*, Vol. 49, No. 3, pp.340–349.

Ghisi, A., Kalicinski, S., Mariani, S., De Wolf, I. and Corigliano, A. (2009b) 'Polysilicon MEMS accelerometers exposed to shocks: numerical-experimental investigation', *Journal of Micromechanics and Microengineering*, Vol. 19, No. 3, pp.035023.

Glaser, S.D. and Tolman, A. (2008) 'Sense of sensing', *Journal of Infrastructure Systems*, Vol. 14, No. 7, pp.4–14.

IEEE Sensors Journal (2009) *Sensor Systems for Structural Health Monitoring*, Vol. 9, No. 11, pp.1319–1321 (Editorial).

International Organization for Standardization (ISO) (2001) 'Fibre-reinforced plastic composites – determination of mode I interlaminar fracture toughness, GIc, for unidirectionally reinforced materials', Standard E, 15024(e).

Kumar, D.N., Raja, S. and Ikeda, T. (2007) 'Active vibration control of smart plates with partially debonded multilayered PZT actuators', *Smart Materials and Structures*, Vol. 16, No. 5, pp.1584–1594.

Mariani, S. and Corigliano, A. (2005) 'Impact induced composite delamination: state and parameter identification via joint and dual extended Kalman filters', *Computer Methods in Applied Mechanics and Engineering*, Vol. 194, No. 50–52, pp.5242–5272.

Mariani, S. and Ghisi, A. (2007) 'Unscented Kalman filtering for nonlinear structural dynamics' *Nonlinear Dynamics*, Vol. 49, Nos. 1–2, pp.131–150.

Mariani, S., Bruggi, M., Caimmi, F., Bendiscioli, P. and De Fazio, M. (2013a) 'Sensor deployment over damage-containing plates: a topology optimization approach', *Journal of Intelligent Material Systems and Structures*, Vol. 24, No. 9, pp.1105–1122.

Mariani, S., Caimmi, F., Eftekhar Azam, S., Bruggi, M. and Bendiscioli, P. (2011) 'Damage detection in vibrating composites using MEMS', *1st International Conference on Urban Construction in the Vicinity of Active Faults*, September 3–5, Tabriz, Iran.

Mariani, S., Corigliano, A., Caimmi, F., Bruggi, M., Bendiscioli, P. and De Fazio, M. (2013b) 'MEMS-based surface mounted health monitoring system for composite laminates', *Microelectronics Journal*, Vol. 44, No. 7, pp.598–605.

Mariani, S., Ghisi, A., Corigliano, A. and Zerbini, S. (2007) 'Multi-scale analysis of MEMS sensors subject to drop impacts', *Sensors*, Vol. 7, No. 9, pp.1817–1833.

Mariani, S., Ghisi, A., Corigliano, A. and Zerbini, S. (2009) 'Modeling impact-induced failure of polysilicon MEMS: a multi-scale approach', *Sensors*, Vol. 9, No. 1, pp.556–567.

Ratcliffe, C., Heider, D., Crane, R., Krauthauser, C., Yoon, M.K. and Gillespie, J.W. (2008) 'Investigation into the use of low cost MEMS accelerometers for vibration based damage detection', *Composite Structures*, Vol. 82, No. 1, pp.61–70.

Salerno, G., Mariani, S., Corigliano, A., Andena, L., Caimmi, F. and Frassine, R. (2010) 'Experimental-numerical assessment of impact-induced damage in cross-ply laminates', Kuczma, M. and Wilmanski, K. (Eds.): *Computer Methods in Mechanics*, ASM 1, Springer-Verlag, Berlin-Heidelberg, pp.493–504.

Schmit, L. and Fleury, C. (1980) 'Structural synthesis by combining approximation concepts and dual methods', *AIAA Journal*, Vol. 18, pp.1252–1260.

STMicroelectronics (2005) *LIS3LV02DQ Datasheet*, Technical Report.

Svanberg, K. (1987) 'Method of moving asymptotes: a new method for structural optimization', *International Journal for Numerical Methods in Engineering*, Vol. 24, No. 2, pp.359–373.

Tao, X., Tang, L., Du, W. and Choy, C. (2000) 'Internal strain measurement by fiber Bragg grating sensors in textile composites', *Composites Science and Technology*, Vol. 60, No. 5, pp.657–669.

Taylor, R.L. (2003) *FEAP – A Finite Element Analysis Program*, Theory Manual, Version 7.5.

Zienkiewicz, O.C. and Taylor, R.L. (2000) *The Finite Element Method*, *Volume II: Solid Mechanics*, 5th ed., McGraw-Hill, London.